Proceedings of ReX'96, the Third International Conference on Recrystallization and Related Phenomena
Edited by Terry R. McNelley
ReX'96 International Advisory Board and Organizing Committee, 1997

181

DYNAMIC RECRYSTALLIZATION IN HIGH STRAIN RATE DEFORMATION

M.A. Meyers*, J.C. LaSalvia*, V.F. Nestorenko, Y.J. Chen and B.K. Kad

*Institute for Mechanics and Materials

Department of Applied Mechanics and Engineering Sciences, University of California - San Diego, 9500 Gilman Dr., LaJolla, CA 92093-0411

ABSTRACT

Large strain, high-strain-rate experiments conducted on copper, titanium, and tantalum, representative of the three most important metallic crystalline structures (FCC, HCP, and BCC, respectively) revealed, in regions of large strain, a microcrystalline structure that is attributed to dynamic recrystallization, enabled by the thermal excursion due to the adiabaticity of the deformation process. These results show that dynamic recrystallization can play a key role in the formation of shear bands, by propitiating the softening mechanism for localization. Two possible mechanisms (migrational and rotational recrystallization) are described and their applicability to the very short duration of the deformation and cooling process (0.02 - 0.2 ms) is discussed.

INTRODUCTION

Adiabatic shear localization, or adiabatic shear band formation, is a phenomenon that has a profound effect on the kinematics of the plastic deformation process. Under special conditions, especially at high strain rates, plastic deformation tends to localize itself in narrow regions with characteristic thicknesses varying from 5 to 200 μm. The high strain rate propitiates adiabaticity or quasi-adiabaticity of the deformation process within these narrow regions. The formation of these bands was first reported by Tresca [1] in the 19th century, and was correctly described by Zener and Hollomon [2] in the 1940's, as being due to the thermal softening becoming greater than work hardening. Shear bands have been identified in a large number of metals and alloys[3-5]. These regions are often precursors to fracture, and are, therefore, very important.

The formation of these bands has been variously attributed to phase transformations ("transformed" bands), or other effects. These various interpretations are due to the absence of obvious metallographic features in many bands. It is only through transmission electron microscopy that the microstructure within shear bands can be revealed.

EXPERIMENTAL OBSERVATIONS

Some of the earliest observations were made by Grebe et al. [6], and by Meyers and Pak [7] on shear bands produced in Ti-6Al-4V and commercial purity titanium, respectively. Figure 1 shows a TEM micrograph of a shear band, observed under an accelerating voltage of 1 MV. The shear band has a thickness of approximately 10 μm and cuts through the micrograph in a diagonal manner. The electron diffraction patterns inside and outside of the shear bands are radically different; outside the

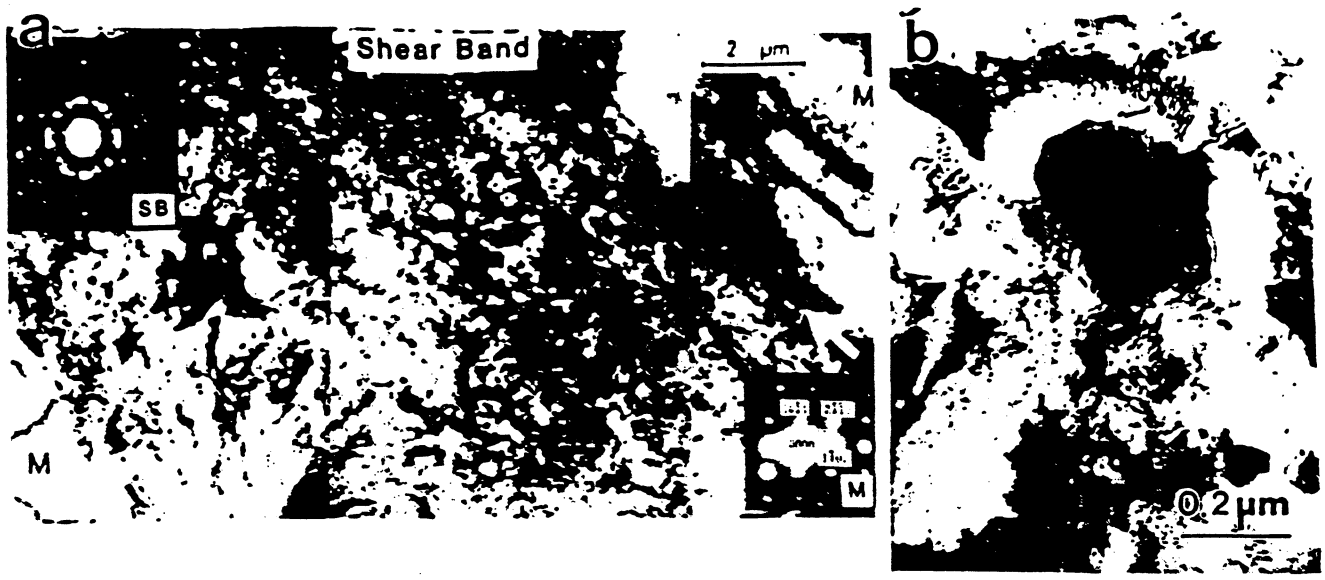

Figure 1 (a) TEM micrograph of shear band in Ti-6Al-4V; (b) Microstructural details within band. (From Meyers and Pak [7]).

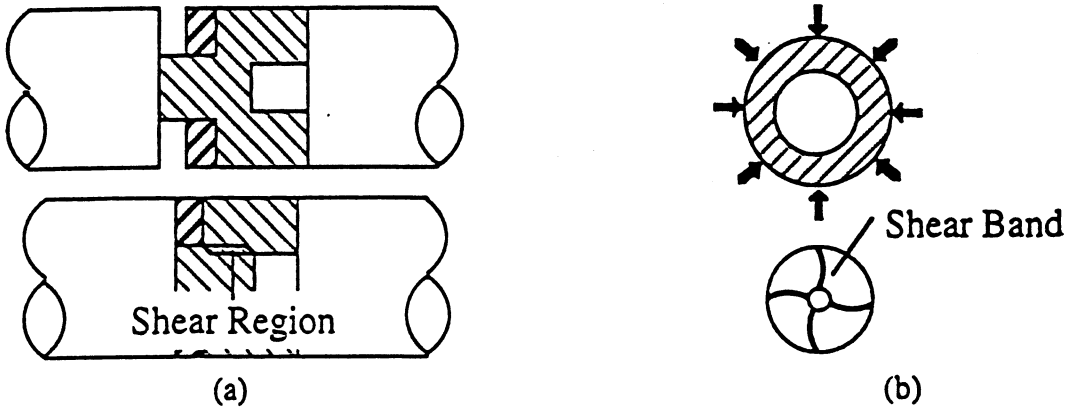

Figure 2 Two experimental techniques applied for large strain, high strain-rate deformation of metals: (a) hat-shaped specimen; and (b) thick-walled cylinder method.

band, the characteristic pattern for a single crystalline orientation is clear. Inside the band, a ring-like pattern, produced by many crystallographic orientations, is apparent. At a higher magnification, the detailed structure inside of the shear band is revealed (Figure 1(b)). It consists of equiaxed grains, with apparent diameters of 0.05 - 0.2 μm. The dislocation density is relatively low. This led to the suggestion by Meyers and Pak [7] that the structure was due to dynamic recrystallization.

The experimental set-up used to generate the shear bands identified in Figure 1 did not produce controlled strain or strain-rate. Hence, quantitative measurement of critical parameters could not be established. The techniques presented in Figure 2 result in the formation of shear bands, under conditions of controlled strain for a known strain rate. The hat-shaped specimen, developed by Meyer and Manwaring [8], was used on titanium [9], copper [10,11], and AISI 4340 steel [12] specimens. The principle of operation is simple. The incident bar impacts the specimen (top of the hat), producing a displacement δ with respect to the bottom of the hat. Plastic deformation takes place in a narrow region between the bottom and top of the hat. The thickness of the spacer ring establishes the displacement δ, and therefore the shear strain γ. The engineering shear strain γ is defined as the

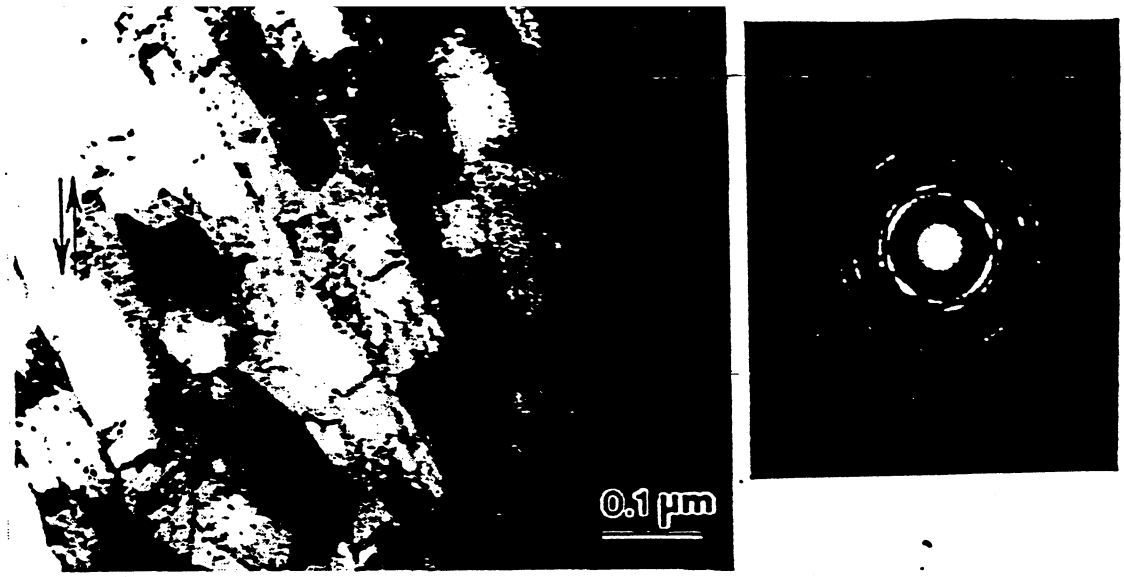

Figure 3 TEM micrograph of microcrystalline structure generated within a shear band in copper (From Andrade et al. [10]).

ratio between the displacement δ, and the thickness w of the shear band. Shear strains of 1 - 4 at shear strain rates > 10^{-4} s^{-1} can be generated. Some materials require higher shear strains to reach the temperatures at which recrystallization occurs. The thick-walled cylinder method, shown in Figure 2(b) is well suited to producing shear strains as high as 10. This technique was developed by Nesterenko and Bondar [13]. A thick-walled cylinder is collapsed radially by energy provided by the detonation of an explosive. The collapse velocity of the central hole can be measured and provides data on the strain rate. The collapse can be arrested at different stages, providing different global strains. The thick-walled cylinder was applied to tantalum [14].

The microscopic observations made within these areas of intense plastic deformation in copper and tantalum are shown in Figures 3 and 4. The microstructures for these different crystal structures are remarkably similar: approximately equiaxed micrograins with diameters between 0.1 and 0.3 μm. The grains have a relatively low dislocation density, and the dihedral angles at grain boundary triple points indicate that the boundaries have energies consistent with high-angles. Three such triple points are marked by arrows. For tantalum, a dark-field micrograph is shown in Figure 4(b), to better illustrate the morphology of the grains. The microstructures shown in Figures 1, 3, and 4 are clearly indicative of recrystallization.

RECRYSTALLIZATION MECHANISM(S)

Since the thermo-mechanical history of the shear localization regions is rather complex, one asks the obvious questions:

a) Do the observed recrystallization features occur during or after plastic deformation?

b) What is the mechanism of recrystallization?

First, calculations will establish for titanium, copper, and tantalum, what plastic strains are required to produce temperatures at which diffusional processes become important; this temperature is set as $0.4T_m$, where T_m is the melting temperature. This can be readily done assuming adiabatic conditions for the deformation process and using a constitutive equation that incorporates strain

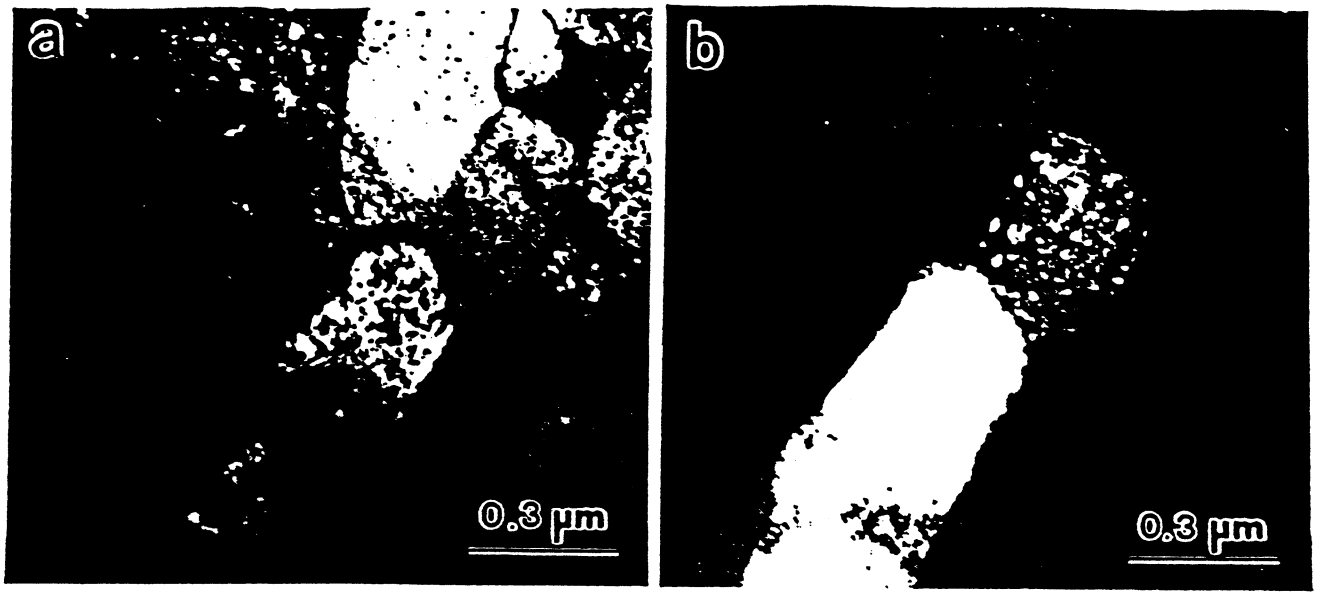

Figure 4 TEM micrographs of microcrystalline structure generated in tantalum. (a) bright field; (b) dark field. (From Nesterenko et al. [14]).

hardening, strain-rate hardening, and thermal softening. One possible constitutive equation, useful due to its simplicity, is the Johnson - Cook [15] equation with modified thermal softening component.

$$\sigma = \left(\sigma_o + k\varepsilon^n\right)\left[1 + C\ln\left(\frac{\dot{\varepsilon}}{\dot{\varepsilon}_o}\right)\right]e^{-\lambda(T-T_r)} \tag{1}$$

where σ_0 is the flow stress at the reference temperature T_r: k and n are strain-hardening parameters; C and $\dot{\varepsilon}_o$ are strain-rate hardening parameters; and λ is a thermal softening parameter. The temperature is obtained from the conversion of the deformation energy to internal energy using the parameter β and integrating:

$$dT = \left(\frac{\beta}{\rho C_p}\right)\sigma d\varepsilon \Rightarrow T = T_o + \frac{1}{\lambda}\ln\left[e^{-\lambda(T_o - T_r)} + \left(\frac{\beta\lambda}{\rho C_p}\right)\left[1 + C\ln\left(\frac{\dot{\varepsilon}}{\dot{\varepsilon}_o}\right)\right]\left[\sigma_o + \left(\frac{k}{n+1}\right)\varepsilon^n\right]\varepsilon\right] \tag{2}$$

The temperatures, normalized with respect the melting temperature, are plotted in Figure 5(a) as a function of plastic strain for titanium, copper, and tantalum. The strains required to reach the recrystallization range are material dependent. For titanium, the value is reached for $\varepsilon = 1.2$; for copper (shock-hardened) the strain is approximately 1.9; and for tantalum, the required strain is much higher, approximately 4.4. The strains generated in the hat-shaped specimen are sufficient to create these favorable thermal regimes for Cu and Ti; for Ta, the thick-walled cylinder method was required. The strain-rate imparted by both methods is fairly similar, approximately $4 \times 10^4\ s^{-1}$.

The cooling times can be estimated from a computational heat-transfer analysis. The results are shown in Figure 5(b). Shear-band thicknesses were taken as 10, 200, and 100 μm for titanium, copper, and tantalum, respectively. If the recrystallized structure forms after deformation, a migrational mechanism is required.

It is possible to estimate the size of the recrystallized grains assuming migrational recrystallization. To a first approximation, it is assumed that the following simple grain growth equation can be used:

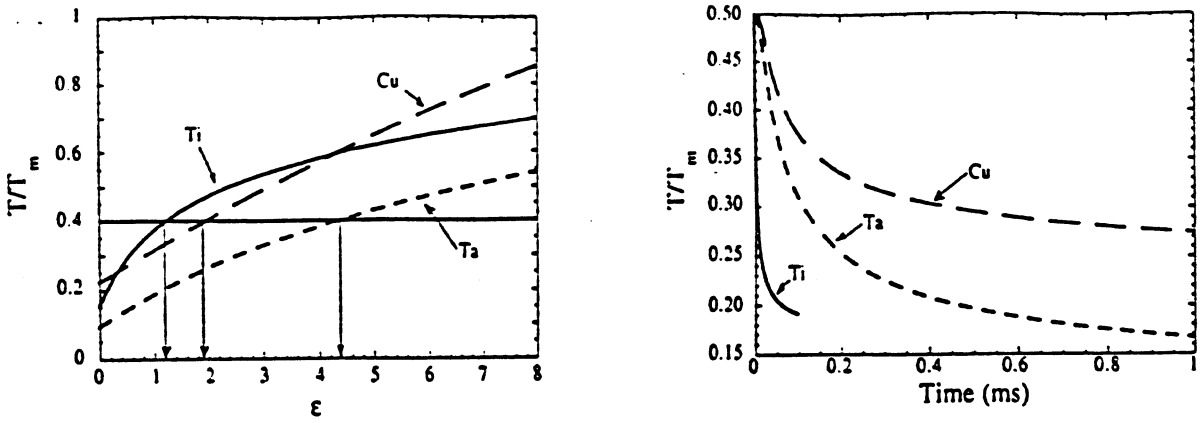

Figure 5 (a) Normalized temperatures as a function of plastic strain for titanium, copper, and tantalum. (b) Shear-band cooling curves for titanium, copper, and tantalum.

$$\Delta d = k_o \Delta t^{1/n} \exp\left(-\frac{Q}{2RT(t)}\right) \qquad d \equiv k_o \sum_{i=0}^{N} \left[\exp\left(-\frac{Q}{2RT(t_i)}\right)\right] \Delta t^{1/n} \qquad (3a,b)$$

where Δd is the change in the instantaneous grain size d, k_o is a rate constant, Q is the activation energy for grain growth, Δt is the change in time t, and T is the absolute temperature. The activation energy for grain boundary migration can be taken as the activation energy for self-diffusion. The pre-exponential factor k_o can be estimated fro experimental results reported in the literature. The exponent n varies between 2 and 10 depending upon impurity content (e.g. n = 2 for ultra pure metals). The final grain size is obtained by numerically integrating Equation (3a). This formalism was applied to the three metals and predicted grain sizes were obtained. The activation energies, pre-exponential factors, and predicted grain sizes are given in Table 1. It can be seen that the calculated grain sizes assuming migrational recrystallization during cooling are inconsistent with the observed results. It is also instructive to establish the deformation time. The deformation time t_f is simply given by the total strain divided by the strain-rate. These times are, respectively, for titanium, copper, and tantalum: 0.4 x 10^{-4}; 0.25 x 10^{-4}; and 10^{-4} s. Only a fraction of this deformation time occurs at a temperature sufficient to induce recrystallization. Hence, the time for recrystallization, t_r, is given by:

$$t_r = t - t_c = t - \frac{\varepsilon_c}{\dot{\varepsilon}} \qquad (4)$$

These time ranges, for the specimens analyzed, are from 0.2 to 0.5 x 10^{-4} s. This time is of the same order as the cooling time. This indicates that a migrational mechanism alone cannot account for the recrystallized structure.

ENERGY ANALYSIS

Derby [16] classifies dynamic recrystallization mechanisms into rotational and migrational types. Rotational recrystallization needs concurrent plastic deformation. It is well documented for geological materials such as quartz [17], halite [18], marble [19], and sodium nitrate [20]. The observations in shear bands of copper [10], tantalum [14] and titanium [9] are suggestive of this mechanism. Figure 6 shows the primary features of the process by which dynamic recrystallization occurs. As can be seen from this figure, a homogeneous distribution of dislocations rearranges

Table 1

Material	k_o	Q (kJ/mol)	n	d (μm)
Cu	-	-	-	-
Ta	19.7	300	10	8.6×10^{-4}
Ti	4.3	322	1	3.9×10^{-4}

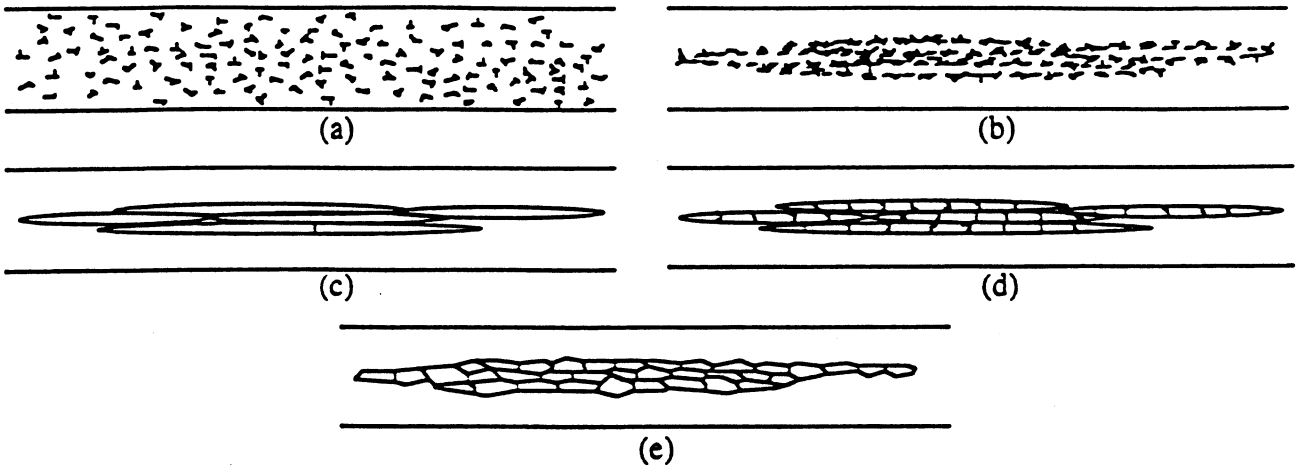

Figure 6 Schematic illustration of microstructural evolution during high-strain-rate deformation. (a) Randomly distributed dislocations; (b) Elongated dislocation cell formation (i.e. dynamic recovery); (c) Elongated subgrain formation; (d) Initial break-up of elongated subgrains; and (e) Recrystallized microstructure.

themselves into elongated dislocation cells (i.e. dynamic recovery). As the deformation continues, these cells become elongated subgrains. Eventually, the elongated subgrains break-up into approximately equiaxed micrograins.

The strain energies per unit volume for dislocation Configurations 1 and 2 (see Figure 6(a) and 6(b)) are given by [21]:

$$E_1 = \left(\frac{A\mu b^2}{4\pi}\right)\rho \ln\left(\frac{\alpha}{2b\rho^{1/2}}\right) \qquad E_2 = \rho\left(\frac{A\mu b^2}{4\pi}\right)\ln\left[\frac{e\alpha}{4\pi b}\left(\frac{S}{V}\right)\frac{1}{\rho}\right] \tag{5, 6}$$

where A is a constant depending upon the character of the dislocation, μ is the shear modulus, b is the magnitude of the Burger's vector, α is a constant which takes in account the core energy of the dislocation, ρ is the dislocation density, e is natural exponent, and S and V are the surface area and volume of the ellipsoid, respectively. The dislocation cell geometry was assumed to be ellipsoidal with aspect ratio is *k*. The cell walls are modeled as tilt boundaries. For an ellipsoid with aspect ratio *k*, the surface area S and volume V are given by:

$$S = 2\pi f(k)W^2 \qquad V = \frac{4}{3}\pi k W^3 \qquad f(k) = 1 + \frac{k^2}{\sqrt{k^2-1}}\sin^{-1}\left(\frac{\sqrt{k^2-1}}{k}\right) \tag{7}$$

where 2W is the cell width.

Equations (5) and (6) give the total energy per unit volume due to the dislocations in Configurations 1 and 2, respectively. Equating these equations gives the following expressions for

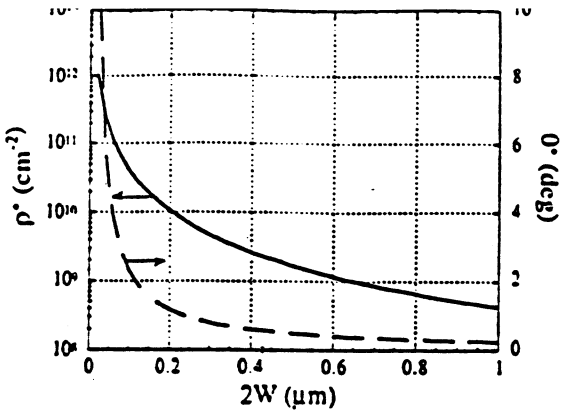

Figure 7 Critical dislocation density ρ^* and resulting misorientation angle θ^* as a function of cell width 2W.

the critical dislocation density ρ^* and misorientation angle θ^* at which Configuration 2 is of lower energy than Configuration 1 :

$$\rho^* = \left[\frac{3e}{4\pi}\left(\frac{f(k)}{k}\right)\left(\frac{1}{W}\right)\right]^2 \qquad \theta^* = \frac{3}{4}\left(\frac{e}{\pi}\right)^2\left(\frac{f(k)}{k}\right)\left(\frac{b}{W}\right) \tag{8a, 9a}$$

It can also be shown that the energy difference between Configurations 1 and 2 is a maximum for $k \rightarrow +\infty$, from which $f(k)/k = \pi/2$. Substitution into Equations (8a) and (9a) gives the following expressions for the critical dislocation density ρ^* and resulting misorientation angle θ^*:

$$\rho^* = \left[\frac{3e}{8}\left(\frac{1}{W}\right)\right]^2 \qquad \theta^* = \frac{3e^2}{8\pi}\left(\frac{b}{W}\right) \tag{8b, 9b}$$

Equations (8b) and (9b) are plotted in Figure 7 as a function of cell width for tantalum (b ≈ 2.333 Å for {112}<111> dislocations). The predicted misorientation angles for the observed cell widths are in excellent agreement with measured values. It is interesting to note that maximum energy difference between Configurations 1 and 2 is given for an aspect ratio $k \rightarrow +\infty$. This is also consistent with observation that once the dislocation cells initially form, they are very long.

These results are consistent with the TEM observations. A typical cell width varies between 0.1 and 0.3 μm, and cell formation occurs at a strain of approximately 1.8, with a temperature rise of 400 K. This corresponds, approximately, to a dislocation density of 10^{10} cm^{-2}, in agreement with predictions.

After the dislocation cells have formed, there must be a net increase in dislocation density as plastic deformation continues. If this increase in dislocation density is primarily accommodated at cell walls, then if cells do not dissociate, the misorientation between cells is expected to increase (consistent with observations). The misorientation angle θ is given by:

$$\theta = \left(\frac{\rho}{\rho^*}\right)\theta^* = \left(\frac{\varepsilon}{\varepsilon^*}\right)\theta^* \tag{10}$$

As observations show, the elongated cells eventually break-up longitudinally. This must be due to a slow down in the cell walls ability to accommodate dislocations. This leads to a reorganization of dislocations into low-energy boundaries perpendicular to the cell walls.

SUMMARY AND CONCLUSIONS

Experimental observations show that the temperature rise during plastic deformation can lead to dynamic recrystallization in Cu (FCC), Ta (BCC), and Ti (HCP) metals. This temperature rise is accomplished by the adiabaticity of the process ensured by high-strain-rate deformation. The recrystallized structure is composed of small, equiaxed grains with 0.1 - 0.5 μm diameter. A rotational mechanism for recrystallization is the most likely process, and is obtained through a microstructural evolution from dislocation cells, elongated subgrains, break-up of subgrains, and finally, to a microcrystalline structure. The energetic calculations are in good agreement with these observations.

This research was sponsored by the National Science Foundation under Grant MSS-902171 and by the U.S. Army Research Office under Contracts DAAL-03-92-G-0108 and DAAH-04-93-G-02611. Support by the Institute for Mechanics and Materials is gratefully acknowledged. This research was conducted in the 1984 - 1996 period and collaboration with H.-r. Pak (Inouie), K.S. Vecchio, and A.H. Chokshi, is greately appreciated. The use of the facilities of the National Center for Electron Microscopy, LBL, is greately appreciated.

REFERENCES

1. M.H. Tresca, Proc. Inst. Mech. Eng., 30, 1878, p. 301.
2. C. Zener and H.H. Hollomon, J. Appl. Phys., 9, 1944, p. 22.
3. H.C. Rogers, Annu. Rev. Mater. Sci., 9, 1979, p. 283.
4. M.A. Meyers, Dynamic Behavior of Materials, J. Wiley, NY, 1994, Chapter xx.
5. Y. Bai and B. Dodd, Adiabatic Shear Localization : Occurrence, Theories, and Applications, Pergamon Press, NY, 1992.
6. H.A. Grebe, H-r. Pak, and M.A. Meyers, Metall. Trans., 13A, 1985, p. 761.
7. M.A. Meyers and H-r. Pak, Acta Metall., 34, 1986, p. 2493.
8. L.W. Meyer and S. Manwaring, in Metallurgical Applications of Shock-Wave and High-Strain-Rate Phenomena (L.E. Murr, K.P. Staudhammer, M.A. Meyers, eds.), Marcel Dekker, NY, 1986, p. 657.
9. M.A. Meyers, G. Subhash, B.K. Kad, and L. Prasad, Mech. Mater., 17, 1994, p. 175.
10. U. Andrade, M.A. Meyers, K.S. Vecchio, and A.H. Chokshi, Acta Metall., 42, 1994, p. 3183.
11. M.A. Meyers, U. Andrade, and A.H. Chokshi, Metall. Mat. Trans. A, 26A, 1995, p. 2881.
12. J.H. Beatty, L.W. Meyer, M.A. Meyers, and S. Nemat-Nasser, in Metallurgical Applications of Shock-Wave and High-Strain-Rate Phenomena (L.E. Murr, K.P. Staudhammer, M.A. Meyers, eds.), Marcel Dekker, NY, 1986, p. 645.
13. V.F. Nesterenko and M.P. Bondar, DYMAT J., 1, 1994, p. 245.
14. V.F. Nesterenko, M.A. Meyers, J.C. LaSalvia, M.P. Bondar, Y.J. Chen, and Y.L. Lukyanov, Mater. Sci. Eng., accepted (1996).
15. G.R. Johnson and W.H. Cook, Proc. 7th Int. Symp. Ballistics, Am. Def. Prep. Ass. (ADPA), Netherlands, 1983.
16. B. Derby, Acta Metall., 39, 1991, p. 955.
17. S. White, Nature, 244, 1973, p. 276.
18. M. Guillope and J.P. Poirier, J. Geoph. Res., 84, 1979, p. 5557.
19. S.M. Schmid, M.S. Paterson, and J.N. Boland, Tectonophysics, 65, 1980, p. 245.
20. PD. Tungatt and F.J. Humphrey, Acta Metall., 32, 1984, p. 1625.
21. J.P. Hirth and J. Lothe, Theory of Dislocations, MacGraw-Hill, 1968, p. 63 and 673.